Dual Control Strategy for Grid-tied Battery Energy Storage Systems to Comply with Emerging Grid Codes and Fault Ride Through Requirements

Maxime Berger, *Member*, *IEEE*, Ilhan Kocar, *Senior Member*, *IEEE*, Evangelos Farantatos, *Senior Member*, *IEEE*, and Aboutaleb Haddadi, *Member*, *IEEE*

***Abstract*—Battery energy storage systems (BESSs) need to comply with grid code and fault ride through (FRT) requirements during disturbances whether they are in charging or discharging mode. Previous literature has shown that constant charging current control of BESSs in charging mode can prevent BESSs from complying with emerging grid codes such as the German grid code under stringent unbalanced fault conditions. To address this challenge, this paper proposes a new FRT-activated dual control strategy that consists of switching from constant battery current control to constant DC-link voltage control through a positive droop structure. The results show that the strategy ensures proper DC-link voltage and current management as well as adequate control of the positive- and negative-sequence active and reactive currents according to the grid code priority. It is also shown that the proposed FRT control strategy is tolerant to initial operating conditions of BESS plant, grid code requirements, and fault severity.**

***Index Terms*—Battery energy storage system, inverter-based resource, fault ride through, electromagnetic transient.**

I. Introduction

ENERGY storage systems (ESSs) provide a key solution for large-scale integration of intermittent renewable resources into power grids [1]. Battery energy storage systems (BESSs) are of particular interest due to their advantages over other storage technologies in terms of energy density, flexibility, and scalability [2], [3]. BESSs are used for performing ancillary functions such as frequency regulation, emergency back-up, voltage regulation, energy time-shifting, capacity optimization, and power quality enhancement [4]-[7].

BESSs are categorized as inverter-based resources (IBRs) [7]. According to fault ride through (FRT) requirements of several grid codes, specific inter-connection requirements of the utility, or emerging standards, e. g., IEEE P2800, bulk power system-connected IBRs are required to remain connected to the grid inside defined limits specified by voltage-versus-time curves and to continue operating as specified during a voltage disturbance. The compliance with these FRT requirements creates an additional control complexity for a BESS compared with wind turbine generators (WTGs) or photovoltaic (PV) that are also IBRs. While WTG and PV systems operate only in inverter mode, a BESS should further comply with FRT requirements in active rectifier mode during battery charging [8], [9].

The behavior of IBRs during FRT operation and their impact on system protection is primarily determined by implemented control strategies and applicable grid code requirements [10]-[12]. Traditional balanced positive-sequence control (BPSC) has been the most common approach used for FRT operation of IBRs. This control entails injecting a positive-sequence reactive current to support grid voltage during disturbances. The lack of negative-sequence current control under BPSC may lead to mis-operation of protective relays, especially negative-sequence quantity-based protections and directional elements [13], [14]. The adoption of negative-sequence current control, e. g., according to VDE-AR-N 4120 Technical Connection Rules (also known as the German grid code) [15], has been shown to reduce the likelihood of such mis-operation events [16]. The implementation of the German grid code requires the use of flexible positive- and negative-sequence control [17].

The FRT operation of grid-tied BESSs has not received the same attention compared with WTG and PV systems. The focus has been rather on enhancing the dynamic performance and FRT capability of WTG systems using storage technologies such as supercapacitors and BESSs [18]-[21]. The short-circuit response of specific protection systems in the presence of grid-tied BESSs is investigated in [22] and [23]. However, important features such as operating mode, i. e., charging or discharging, internal control strategies, and grid code requirements are not presented. Some of these details are discussed in [24] and [25]. However, the investigation is limited to single-stage topology, i. e., without a DC-DC interface and the use of BPSC. The management of the DC-link during a fault is not discussed in [22]-[25].

Practical grid-tied BESS plants are based on the two-stage

Manuscript received: March 17, 2021; revised: May 21, 2021; accepted: September 10, 2021. Date of CrossCheck: September 10, 2021. Date of online publication: October 29, 2021.

M. Berger and I. Kocar (corresponding author) are with the Department of Electrical Engineering, Polytechnique Montréal, Montréal, Canada (e-mail: maxime.berger@polymtl.ca; ilhan.kocar@polymtl.ca).

E. Farantatos and A. Haddadi are with the Electric Power Research Institute (EPRI), Palo Alto, USA (e-mail: efarantatos@epri.com; ahaddadi@epri.com).

DOI: 10.35833/MPCE.2021.000182

topology to increase the system scalability. They are composed of multiple bidirectional DC-DC converter (BDC) units in parallel interfaced with a common DC-link. This enables integrating multiple battery sources through a common grid-side converter (GSC) DC-AC interface with the power grid [26]. Reference [27] demonstrates that the use of a two-stage topology as well as the use of a flexible positive- and negative-sequence control strategy both brings additional constraints on the BESS control, and that proper DC-link management during a fault is critical. Inadequate DC-link regulation can prevent BESS plants from riding through faults and further complying with grid code requirements [28]. It is also demonstrated that a fault occurring during the conventional constant battery charging phase [29] is the most stringent scenario on both DC-link voltage regulation and grid voltage support. The use of a flexible positive- and negative-sequence control scheme compliant with the German grid code under stringent unbalanced faults aggravates the situation further. A solution is proposed in [27] to switch the BDC control from constant current charging to DC-link voltage regulation during grid faults in charging mode. However, the solution proposed in [27] does not consider practical plant constraints such as parallel operation of BDC units as well as the impact of initial operating conditions of BESS plant, e. g., battery state-of-charge (SOC) and active power set-point, and grid code requirements.

This paper proposes a new FRT control strategy for practical BESS plants to comply with the German grid code in charging mode. A detailed simulation model in EMTP is built to validate the proposed control strategy. This model includes experimentally validated scalable models of li-ion battery, converters, and generic control strategies accounting for the non-linear effect of current limiters and grid code priority logic. The schematic of BESS model for FRT control strategy with parallel-connected BDC units is shown in Fig. 1, where i_b is the battery current; e_b is the battery internal voltage; R_s is the battery internal resistance; v_{dc} is the DC-link voltage; v_{dc}^{ref} is the initial DC-link reference voltage; v_b is the battery terminal voltage; i_{dc} is the BDC input current in charging mode; P_{BESS} is the nominal power of each BESS unit; N_{BESS} is the number of BESS units in the BESS plant; N_{BDC} is the number of aggregated BDC units in parallel on the DC-link; i_b^{ref} is the reference battery current; $\Delta V'$ is the output of the BESS plant level controller calculated to regulate the reactive power at the point of interconnection (POI); Q'_{poi} is the reactive power at the POI; I_{poi} and V_{poi} are the current and voltage at the POI, respectively; i_{dg}^{ref+} is the pre-fault positive-sequence active reference current value at FRT activation such that the BESS plant maintains the charging current if permitted by the limiter with a priority logic algorithm; v_{dc}^{min} is the minimum DC-link reference voltage; d is the duty cycle of the BDC current controller; PI stands for proportional integral; PLL stands for phase locked loop; and LV, MV, and HV stand for low voltage, medium voltage, and high voltage, respectively.

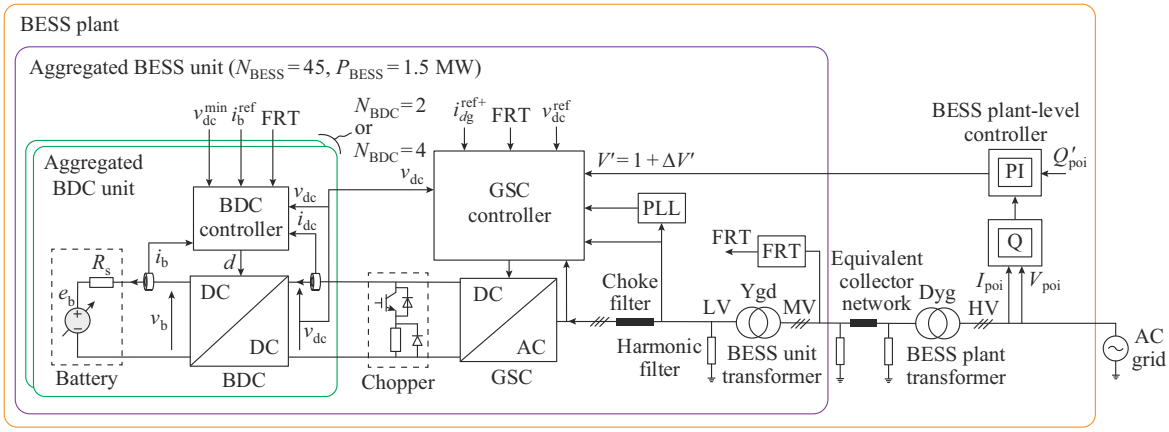

Fig. 1. Schematic of BESS model for FRT control strategy with parallel-connected BDC units.

Key improvements to the solution presented in [27] are also proposed. First, this paper proposes a positive droop-based solution for proper DC-link management with parallel-connected BDC units. Furthermore, it proposes an improved GSC control strategy considering grid code requirements to ensure the required magnitude of negative-sequence reactive current and grid voltage support, and that lowest priority is given to the positive-sequence active current. The positive-sequence active current control strategy of the GSC is also coordinated with the BDC control scheme through a new limiter logic as well as two FRT-activated bumpless structures that ensure controlled transition at fault inception and fault removal. The proposed FRT control strategy is analyzed in terms of its performance on the DC-link management, and positive- and negative-sequence current control. It is demonstrated that the strategy is tolerant to the operating conditions of BESS plant (SOC and active power set-point), grid code requirements (reactive current injection), and fault severity (close fault v.s. remote fault).

II. Proposed BESS Fault Management Strategy

A. Investigated System Topology

The BESS plant structure can be divided into two main categories depending on the number of conversion stages of power electronics used between the battery and AC grid [1], [7].

The single-stage topology consists of a battery directly connected to the DC-link and a GSC DC-AC interface with the power grid. This topology is simple and of low-cost and provides the maximum efficiency. However, it is less flexible in terms of control, and it significantly increases the stress on the battery under both normal and fault conditions [27].

The two-stage topology provides increased flexibility and scalability by introducing an intermediate BDC for interfacing the battery with the DC-link. The BDC enables a more precise control of the DC-link voltage, battery voltage, and battery current. While this topology reduces the overall efficiency of the BESS plant, it significantly reduces the stress on the battery. This structure is also scalable and provides redundancy [3].

The coordination between the GSC and BDC control strategies is necessary which leads to additional control constraints. These constraints must be managed under grid fault conditions, otherwise, they can prevent BESSs from riding through faults. To increase the capacity and system adaptability, the two-stage topology can be expanded by paralleling the BDC, GSC, or BESS unit transformer outputs.

The BESS plant model used in this paper is an aggregated version of the two-stage topology with parallel BESS unit transformer output, as shown in Fig. 1. The BESS plant model is flexible and allows paralleling multiple aggregated BDC units on the same DC-link, which, as demonstrated in this paper, is important to evaluate the potential interactions between the BDC units and the GSC interface under grid fault conditions. The BESS plant is connected to an HV transmission network through an MV equivalent collector network and BESS plant transformer.

B. Statement of Problem

During the conventional constant charging current phase, severe transient voltage drop $v_{\mathrm{dc,min}}$ and steady-state voltage drop $v_{\mathrm{dc,ss}}$ on the DC-link can prevent BESS plants from complying with grid code requirements [28]. This problem is explained using the ideal representation in Fig. 2, where $V_{\mathrm{dc,on}}$ is the chopper-on voltage; $V_{\mathrm{dc,off}}$ is the chopper-off voltage; i_{b}' is the BDC inner loop reference current; i_{dg}^{+} and i_{qg}^{+} are the positive-sequence active and reactive currents of GSC, respectively; and i_{dg}^{-} and i_{qg}^{-} are the negative-sequence active and reactive currents of GSC, respectively.

The voltage drop is caused by the limitations on i_{dg}^{+} due to the required injections of i_{qg}^{+}, i_{dg}^{-}, and i_{qg}^{-}, which leads to a reduction in the injected DC current i_{gsc} on the DC-link as shown in Fig. 3, where v_{dg}^{+} is the instantaneous positive-sequence voltage at the GSC AC terminals; L_{b} is the filter inductor; P_{b} is the initial power for each battery; Q_1 and Q_2 are the transistors; and C_{dc} is the DC-link capacitor. This can bring the BDC controller into saturation such that i_{b} decreases in an uncontrolled manner until v_{dc} sufficiently decreases to achieve power balance on the DC-link.

The problem of DC-link regulation is aggravated by the use of a flexible positive- and negative-sequence control scheme compliant with [15] due to the required i_{dg}^{-} and i_{qg}^{-}, which further limits i_{dg}^{+} under unbalanced fault conditions.

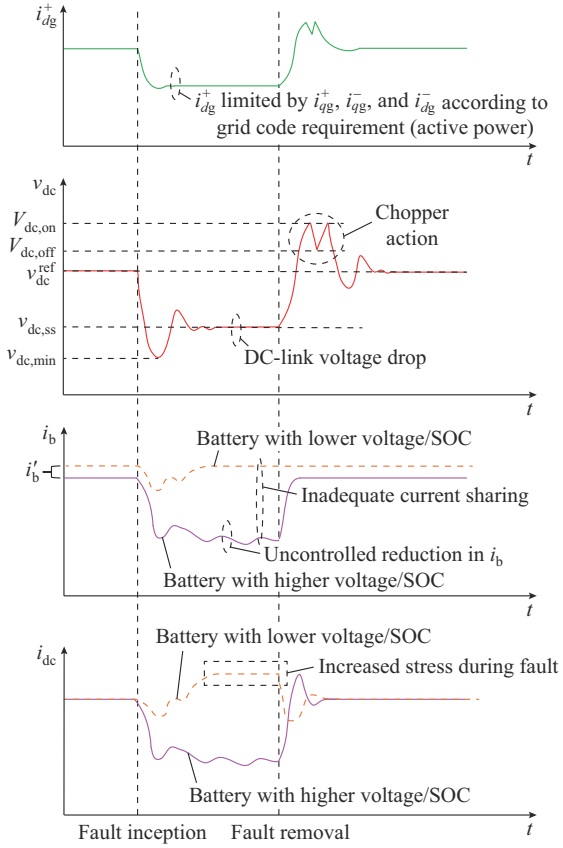

Fig. 2. Ideal representation of problem of DC-link regulation with conventional BDC constant charging current control and parallel-connected BDC units' topology under stringent grid fault condition.

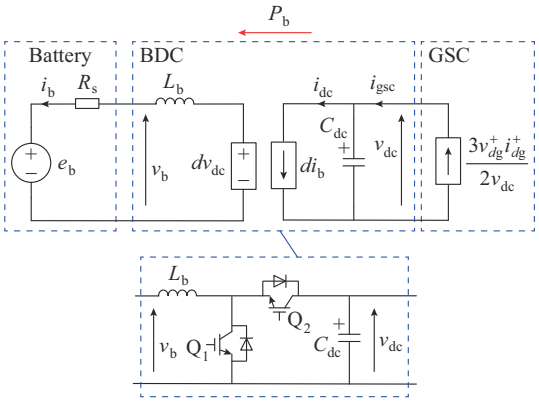

Fig. 3. Equivalent schematic of BDC unit with battery and GSC interfaces in charging mode.

For the same power level of the BESS plant p_0, $v_{\mathrm{dc,min}}$ is also more severe for a close fault than for a remote fault, which is explained by the larger power drop at the AC grid [27]. Furthermore, it is also shown in [27] that both $v_{\mathrm{dc,min}}$ and $v_{\mathrm{dc,ss}}$ are impacted by the battery characteristics and that the voltage drop is more severe for low SOC and low battery nominal voltage V_{n}.

Voltage drop dependency on battery characteristics is explained using the simplified equivalent schematic in Fig. 3. Under the fault conditions in the charging mode, if i_{gsc} is insufficient to support the constant i_{dc} drawn by the BDC, v_{dc}

will rapidly drop and d will rapidly saturate to its maximum value. For the sake of simplicity, it is assumed that the maximum duty cycle value is $d=1$. This means that transistor Q_2 is always ON in Fig. 3, such that the battery becomes directly connected to the DC-link. Under such a condition, v_{dc} will follow the relationship below [27]:

$$v_{dc}=\left(e_b+\sqrt{e_b^2+6R_s v_{dg}^+ i_{dg}^+}\right)\Big/2 \tag{1}$$

This suggests that when i_{dg}^+ decreases with v_{dg}^+ constant, which is dependent on fault location, v_{dc} decreases. This effect is weighted by R_s. Furthermore, according to the battery model defined in Section II-D, e_b is a function of the battery model parameters, and in particular, the battery SOC and V_n.

As shown in Fig. 2, the problem with the saturation of the BDC controller can also lead to an inadequate DC-link current management when multiple BDC units are operated in parallel. Batteries can be at different SOCs and have slightly different characteristics due to manufacturing tolerances, ageing, and operating conditions, which can lead to inadequate current sharing between the parallel BDC units and result in increased stress during the fault.

Furthermore, at fault removal, transient overvoltage also occurs because the BDC units cannot instantaneously transfer the active power injected from the GSC to the batteries. This can require the use of the chopper if the overvoltage condition is too severe and exceeds its turn-on voltage threshold $V_{dc,on}$, as shown in Fig. 2.

C. Proposed FRT Control Strategy

As shown in Fig. 4, the proposed FRT control strategy consists of adapting the controls of the BDC units and GSC upon receiving an FRT activation signal, which is determined through the measurement of the voltage at the MV side of the BESS plant as shown in Fig. 1.

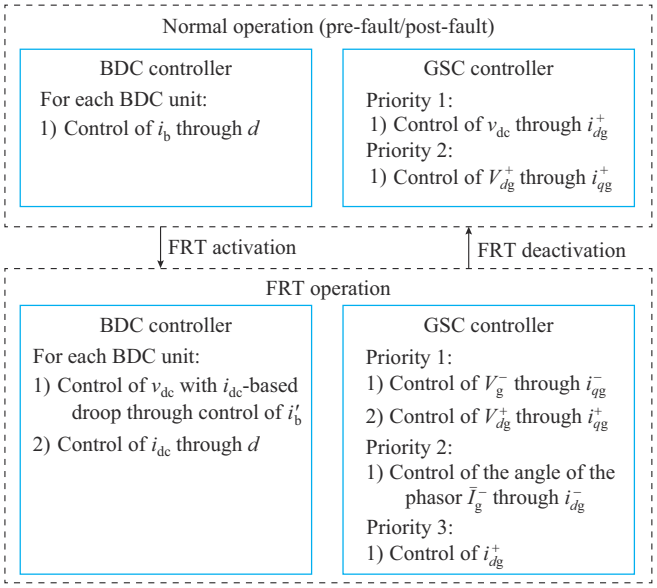

Fig. 4. Flow chart of proposed FRT control strategy of BESS plant.

In Fig. 4, V_g^- is the magnitude of the negative-sequence voltage phasor; and I_g^- is the magnitude of the negative-sequence current phasor. At fault inception, the FRT activation signal is activated when the voltage decreases below the pickup voltage, and at fault removal, the FRT activation signal is deactivated when the voltage rises above the reset voltage.

Upon receiving the FRT activation signal, all the BDC units switch from constant i_b control to constant v_{dc} control through a droop structure based on measuring i_{dc} of the BDC units. This permits current sharing between the BDC units while regulating v_{dc} during FRT. Simultaneously, the GSC switches from constant v_{dc} control to constant i_{dg}^+ control. The control priority is equally given to i_{qg}^- and i_{qg}^+ according to grid code priority. The control of i_{dg}^+ has the lowest priority. When the grid voltage returns above the FRT reset voltage, the BDC and GSC controllers automatically revert to their normal operation controls.

D. Li-ion Battery Model

The behavior of a BESS plant, as can be observed from POI during a grid fault, should ideally be independent of the battery internal parameters such as the battery SOC. The most relevant battery characteristics are included in this paper to confirm that the proposed control strategy is tolerant to battery internal characteristics.

The aggregated li-ion battery model implemented in this paper is a modified version of the generic model proposed and experimentally validated in [30]. This model has been previously presented and validated against manufacturer's data in [27] and further modified considering multiple aggregated BDC units in parallel. The terminal voltage of each battery is given by:

$$v_b=e_b-R_s i_b \tag{2}$$

e_b is calculated in charging operation by:

$$e_b=E_0-K\frac{Q_n}{Q_n+0.1\cdot it}i_b^*-K\frac{Q_n}{Q_n-it}\cdot it+A\mathrm{e}^{-B\cdot it} \tag{3}$$

where E_0 is the battery constant voltage; K is the polarization constant; $it=\int i\mathrm{d}t$ is the battery charge level; i_b^* is the filtered battery current obtained by filtering i_b through a first-order low-pass filter with a time constant of 30 s as defined in [30]; A is the exponential zone amplitude; Q_n is the nominal battery capacity; and B is the inverse exponential zone time constant.

The aggregated model parameter values are scaled based on Q_n and V_n as follows:

$$\begin{cases} A=k_A V_n \\ B=k_{B1}Q_n+k_{B2} \\ K=k_K\left(V_n/Q_n\right) \\ R_s=k_{Rs}\left(V_n/Q_n\right) \\ E_0=k_{E0}V_n \end{cases} \tag{4}$$

where k_A, k_{B1}, k_{B2}, k_K, k_{Rs}, and k_{E0} are selected to best match the performance data given by cell manufacturers.

Q_n is scaled using the BESS plant-level information as:

$$Q_n=\left[\left(N_{BESS}/N_{BDC}\right)P_{BESS}T_n\right]\Big/V_{dc} \tag{5}$$

where T_n is the total discharge time in hours to extract the total battery capacity Q_n if the battery is discharged at a current of $I_n = Q_n/T_n$; and V_{dc} is the nominal DC-link voltage.

P_b is calculated by:

$$P_b = N_{BESS} P_{BESS} p_{BDC} \tag{6}$$

where $p_{BDC} = p_0/N_{BDC}$ is the initial power reference of each BDC unit. The battery SOC is dynamically calculated as:

$$SOC = \left(1 - \frac{it}{Q_n}\right) \times 100\% \tag{7}$$

As shown in Fig. 1, the BESS plant investigated in this paper has 45 BESS units ($N_{BESS} = 45$) with $P_{BESS} = 1.5$ MW. The total nominal power is 67.5 MW. For the purpose of validation of the FRT control strategy with parallel-connected BDC units, the total active power of the BESS plant is either divided into two or four aggregated BDC units, i. e., $N_{BDC} = 2$ or $N_{BDC} = 4$, as shown in Fig. 1.

E. Analysis of BDC Model

1) BDC Model

The topology considered in this paper is the non-isolated two-switch buck-boost. The equivalent schematic diagram of the BDC average value model with battery and GSC interfaces in charging mode is shown in Fig. 3. The charging mode operates in buck mode with Q_1 being open. The duty cycle d of the pulse width modulation (PWM) control signal applied to Q_2 is determined by the BDC controller, as shown in Fig. 5(a). In Fig. 5, v'_{dc} is the DC-link reference voltage; K_p and K_i are the gains; R_d is the droop resistance; e_v is the error on DC-link voltage; u_i is the integrator output; and u is the PI controller output.

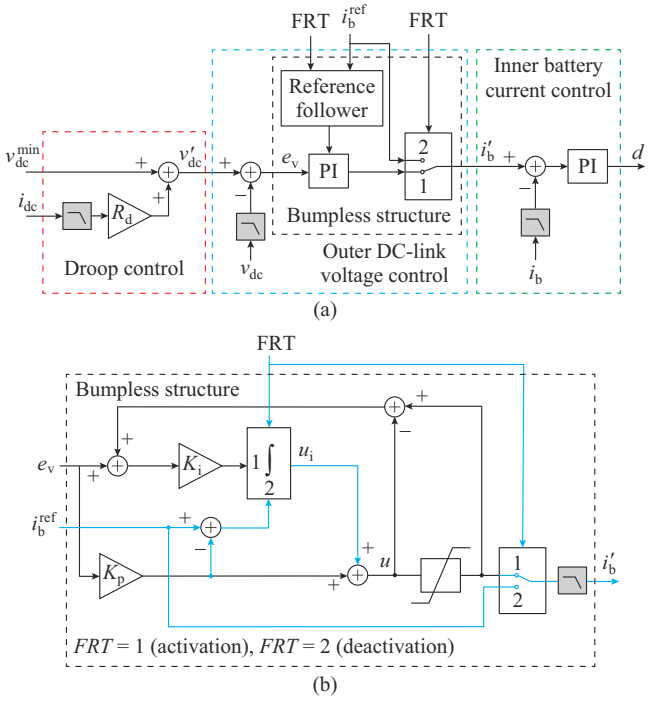

Fig. 5. Proposed BDC control strategy in active state of FRT. (a) Simplified representation of control scheme. (b) Detailed representation of bumpless structure.

As can be observed from the DC-link, the GSC is acting as controlled current i_{gsc}, which depends on v_{dg}^+ and i_{dg}^+ as well as v_{dc}. i_{gsc} does not depend on i_{qg}^+ due to the selected PLL control reference ($v_{qg}^+ = 0$).

The proper control of the BDC units is mandatory for adequate management of the DC-link during FRT operation of the BESS plant. The sizing of the BDC controller requires deriving its small-signal average model for defining the control-to-output transfer functions. It requires deriving the operating point in steady state based on the battery model and BESS plant-level parameter values. In steady state, $e_b = E_b$, $v_b = V_b$, $i_b = I_b$, $i_{gsc} = I_{gsc}$, $v_{dc} = V_{dc}$, $d = D$, and $D' = 1 - D$. With P_b for each battery calculated in (6), the operating point of each BDC unit in parallel is calculated as [27]:

$$I_b = \left(DV_{dc} - E_b\right) \Big/ R_s \tag{8}$$

$$D = \left(E_b + \sqrt{\Delta}\right) \Big/ \left(2V_{dc}\right) \tag{9}$$

$$\Delta = E_b^2 + 4V_{dc} R_s I_{gsc} \tag{10}$$

$$I_{gsc} = P_b / V_{dc} \tag{11}$$

The small-signal model of the buck converter with battery as a load is given with the standard state-space formulation, and the symbol ˆ represents the regression value:

$$\mathrm{d}\hat{\boldsymbol{x}}/\mathrm{d}t = \hat{\boldsymbol{A}}\hat{\boldsymbol{x}} + \hat{\boldsymbol{B}}\hat{\boldsymbol{u}} \tag{12}$$

$$\hat{\boldsymbol{y}} = \hat{\boldsymbol{C}}\hat{\boldsymbol{x}} + \hat{\boldsymbol{D}}\hat{\boldsymbol{u}} \tag{13}$$

where

$$\begin{cases} \hat{\boldsymbol{x}} = \begin{bmatrix} \hat{v}_{dc} \\ \hat{i}_b \end{bmatrix} \\ \hat{\boldsymbol{u}} = \begin{bmatrix} \hat{d} \\ \hat{i}_{gsc} \end{bmatrix} \\ \hat{\boldsymbol{y}} = \begin{bmatrix} \hat{v}_{dc} \\ \hat{i}_b \end{bmatrix} \end{cases} \tag{14}$$

$$\begin{cases} \hat{\boldsymbol{A}} = \begin{bmatrix} 0 & \dfrac{-D}{C_{dc}} \\ \dfrac{D}{L_b} & \dfrac{-R_s}{L_b} \end{bmatrix} \\ \hat{\boldsymbol{B}} = \begin{bmatrix} \dfrac{-I_b}{C_{dc}} & \dfrac{1}{C_{dc}} \\ \dfrac{V_{dc}}{L_b} & 0 \end{bmatrix} \\ \hat{\boldsymbol{C}} = \begin{bmatrix} 1 & 0 \\ 0 & 1 \end{bmatrix} \\ \hat{\boldsymbol{D}} = \begin{bmatrix} 0 & 0 \\ 0 & 0 \end{bmatrix} \end{cases} \tag{15}$$

2) Proposed BDC FRT Control Strategy

As previously described in Section II-B, during a grid fault with the BESS in charging mode, significant DC-link voltage drop can occur if the BDC units are operated with conventional constant charging current control. The voltage drop is a function of battery parameters such as V_n, R_s, and

SOC. Furthermore, if multiple BDC units are operated on the same DC-link in parallel, the saturation of the BDC controllers can lead to inadequate DC-link current management.

In this paper, it is proposed to enable the cascade control of v_{dc} through the control of i_b, during FRT, as shown in Fig. 5(a). However, for multiple BDC units in parallel, it is also necessary to ensure coordinated control between the units to ensure stability and acceptable current sharing during FRT. Since the BDC units are acting as loads, as can be observed from the DC-link, it is proposed to implement a positive droop control feature, as shown in Fig. 5(a).

Droop control is used to control v'_{dc} as a function of the measured input charging current i_{dc}. Droop control is particularly important to ensure proper sharing of the current between the BDC units in presence of discrepancies on voltage feedback measurements. As shown in Fig. 6, the main parameters of the droop structure are v_{dc}^{min}, the maximum DC-link reference voltage v_{dc}^{max}, and R_d. The value setting of v_{dc}^{min} should consider the minimum permissible DC-link voltage for small values of i_{dc}, and R_d must be high enough to ensure proper sharing with the maximum expected tolerances on the voltage feedback measurements. For a fixed value of v_{dc}^{min}, the value of R_d should also be limited to ensure that there is no overvoltage on the DC-link for high levels of i_{dc}. The necessity of the droop control with proper settings will be demonstrated in Section III-C.

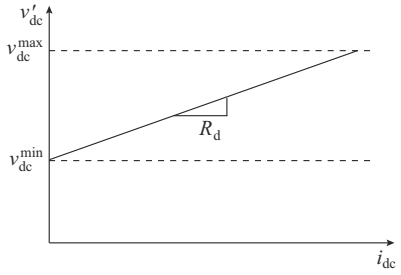

Fig. 6. Droop control for DC-link voltage regulation with parallel-connected BDC units during FRT.

The controller automatically resumes constant battery current control once the FRT controller detects that the grid voltage returns within the limits. The controller features a bumpless structure to ensure a controlled transition from current to voltage control, and vice versa. Prior to fault ($FRT=2$), the output of u_i is maintained to $i_b^{ref}-K_p e_v$ such that u follows i_b^{ref} to avoid discontinuity on i'_b at FRT activation ($FRT=1$). The output low-pass filter ensures smooth transition of the reference current when the controller returns to $i'_b=i_b^{ref}$ at FRT deactivation ($FRT=2$).

To calculate the parameter values of inner current controller, the transfer function between $\hat{i}_b$ and d is extracted from (12) - (15). For the outer voltage control loop, the transfer function between the DC-link voltage $\hat{v}_{dc}$ and the battery reference current $\hat{i}'_b$ is determined by assuming that the dynamic of i_b is much faster than the dynamic of v_{dc} following the design procedure presented in [31] with $R_g=V_{dc}/I_{gsc}$.

$$\hat{v}_{dc}/\hat{i}'_b = DR_g/\left(sC_{dc}R_g+1\right) \tag{16}$$

F. Proposed GSC Control Strategy

As shown in Fig. 1, BESS plants typically have a plant-level controller that permits the control of either the reactive power or voltage, or power factor at the POI, which is similar to wind parks [32] - [34]. This is important for determining the initial operating point of the BESS plant at fault inception.

The proposed GSC control strategy for FRT of the BESS plant in charging operation under flexible positive- and negative-sequence control compliant with [15] is presented in Fig. 7, where i'^{+}_{dg} and i'^{+}_{qg} are the positive-sequence active and reactive reference currents of GSC, respectively; K_{V+} and K_{V-} are the positive- and negative-sequence voltage regulator gains, respectively; i''^{+}_{dg} and i''^{+}_{qg} are the revised positive-sequence active and reactive reference currents, respectively; i''^{-}_{dg} and i''^{-}_{qg} are the revised negative-sequence active and reactive reference currents, respectively; V^{-}_{dg} and V^{-}_{qg} are the d- and q-axis components of V^{-}_{g}, respectively; and V^{+}_{dg} is the grid voltage of GSC.

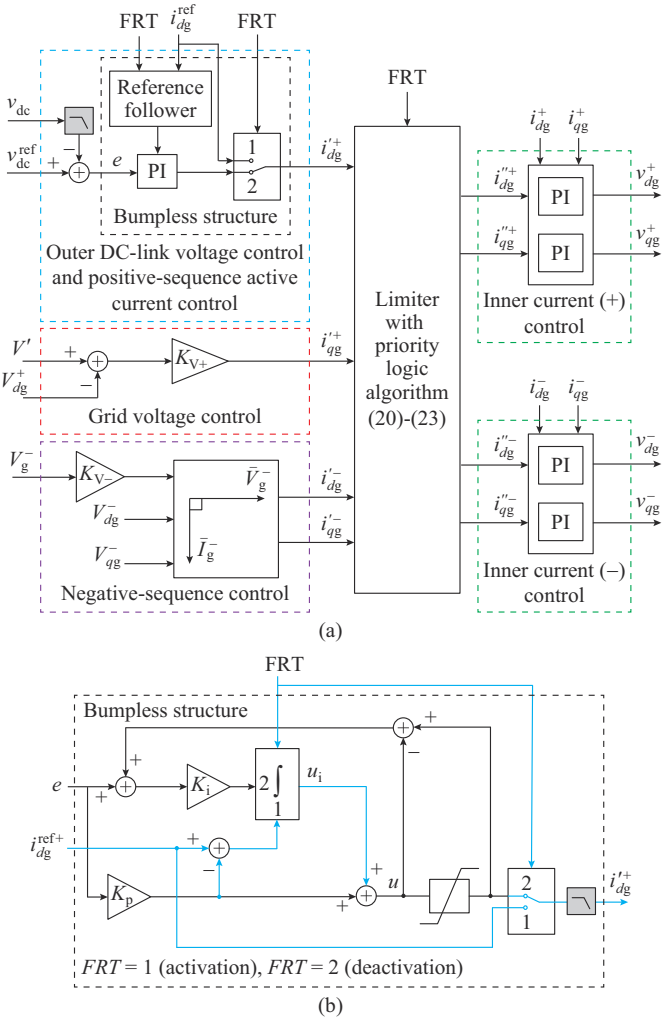

Fig. 7. Proposed GSC control strategy in active state of FRT. (a) Simplified representation of control scheme. (b) Detailed representation of bumpless structure.

Prior to a fault, the BDC units are operated with constant battery charging current control and the GSC regulates v_{dc}

by controlling i'^{+}_{dg}. The GSC also controls V^{+}_{dg} through i'^{+}_{qg} calculated as [10]:

$$i'^{+}_{qg} = K_{V+}\left(1 + \Delta V' - V^{+}_{dg}\right) \tag{17}$$

In normal operation, the priority is given to the active (*d*-axis) current for a proper DC-link voltage control. In this paper, the network is assumed to be balanced such that $i'^{-}_{dg} = i'^{-}_{qg} = 0$ prior to a fault.

During FRT, the BDC controller switches to constant v_{dc} control, as presented in Section II-E. In this case, the GSC stops regulating v_{dc} and changes to constant i^{+}_{dg} control. The proposed GSC control strategy limits the adverse impact of the consumption of i^{+}_{dg} on the ability of the BESS plant to support grid voltage while ensuring the minimum possible perturbation on the DC-link. This is achieved by controlling i^{+}_{dg} to be the maximum value permitted by the limiter with a priority logic algorithm. The impact of i^{+}_{dg} control on DC-link voltage regulation and grid voltage support with BESSs in charging mode is discussed in [28].

Under flexible positive- and negative-sequence control compliant with [15], the GSC regulates i^{+}_{dg}, i^{+}_{qg}, i^{-}_{dg}, and i^{-}_{qg}. During an unbalanced fault, the negative-sequence reactive reference current i'^{-}_{qg} is calculated to be proportional to V^{-}_{g} [10]:

$$i'^{-}_{qg} = K_{V-}V^{-}_{g} \tag{18}$$

where $K_{V-} = 2, 3, \ldots, 6$ according to the grid code requirements [15]; and V^{-}_{g} is defined as:

$$V^{-}_{g} = \sqrt{\left(V^{-}_{dg}\right)^2 + \left(V^{-}_{qg}\right)^2} \tag{19}$$

During a grid fault, the reference for the injection of i'^{+}_{qg} is determined by (17). The priority is given to the injection of i^{+}_{qg} and i^{-}_{qg} for grid voltage support and reduction of negative-sequence voltage, respectively. The control of i^{+}_{qg} and i^{-}_{qg} is defined such that they both have the same priority level over the *d*-axis currents. The reactive reference currents are limited when $\left|i'^{+}_{qg}\right| + \left|i'^{-}_{qg}\right| > I^{\lim}_{qg}$ by revising their values with [32]. i''^{+}_{qg} and i''^{-}_{qg} are calculated as:

$$\begin{cases} i''^{+}_{qg} = i'^{+}_{qg}\left[\dfrac{I^{\lim}_{qg}}{\left|i'^{+}_{qg}\right| + \left|i'^{-}_{qg}\right|}\right] \\ i''^{-}_{qg} = i'^{-}_{qg}\left[\dfrac{I^{\lim}_{qg}}{\left|i'^{+}_{qg}\right| + \left|i'^{-}_{qg}\right|}\right] \end{cases} \tag{20}$$

where $I^{\lim}_{qg}$ is the total current limit specified in the *q*-axis.

The negative-sequence active reference current i'^{-}_{dg} is then calculated to ensure that the phasor $\bar{I}^{-}_{g}$ is ideally 90° phase-shifted from the phasor $\bar{V}^{-}_{g}$ such that the GSC absorbs purely reactive power in the negative-sequence frame. However, the current in the *d*-axis is limited by the level of reactive currents required in the *q*-axis in (20). The maximum available active current in the *d*-axis $i^{\lim}_{dg}$ is dynamically calculated as [32]:

$$i^{\lim}_{dg} = \sqrt{\left(I^{\lim}_{g}\right)^2 - \left(\left|i''^{+}_{qg}\right| + \left|i''^{-}_{qg}\right|\right)^2} \tag{21}$$

where $I^{\lim}_{g}$ is the total current limit specified at the terminal of the GSC. The limiter with priority logic algorithm dynamically limits the magnitude of negative-sequence active current in the *d*-axis i'^{-}_{dg} as follows:

$$\left|i''^{-}_{dg}\right| = \min\left(\left|I^{\lim}_{dg}\right|, \left|i^{\lim}_{dg}\right|, \left|i'^{-}_{dg}\right|\right) \tag{22}$$

where $I^{\lim}_{dg}$ is the total current limit specified in the *d*-axis. The control of i^{-}_{dg} has also the priority over the positive-sequence active current i^{+}_{dg}, such that the available charging current i_{gsc} naturally decreases following the requested demands in i^{+}_{qg}, i^{-}_{qg}, and i^{-}_{dg}. This ensures the minimum perturbation in the system while prioritizing grid code requirements. The proposed GSC control strategy permits controlling the positive-sequence active current i^{+}_{dg} during FRT, but it is dynamically limited as:

$$\left|i''^{+}_{dg}\right| = \min\left(\min\left(\left|I^{\lim}_{dg}\right|, \left|i^{\lim}_{dg}\right|\right) - \left|i''^{-}_{dg}\right|, \left|i^{\text{ref}+}_{dg}\right|\right) \tag{23}$$

As shown in Fig. 7, i''^{+}_{dg}, i''^{+}_{qg}, i''^{-}_{dg}, and i''^{-}_{qg} are then regulated by inner controllers. The GSC outer DC-link voltage controller automatically resumes to constant DC-link voltage control once the FRT controller detects that the grid voltage returns within the limits. The GSC outer DC-link voltage controller also features a bumpless structure for the controlled transitions at FRT activation and deactivation. The output low-pass filter ensures smooth transition of the reference current when the controller transitions from v_{dc} control ($FRT = 2$) to constant current control with $i'^{+}_{dg} = i^{\text{ref}+}_{dg}$ at FRT activation ($FRT = 1$). During a fault, u_i is maintained to $i^{\text{ref}+}_{dg} - K_p e$ such that u follows $i^{\text{ref}+}_{dg}$ to avoid the discontinuity on i'^{+}_{dg} at FRT deactivation ($FRT = 2$).

G. Test Network

The proposed FRT control strategy is validated using the 120 kV/60 Hz transmission network shown in Fig. 8 [27].

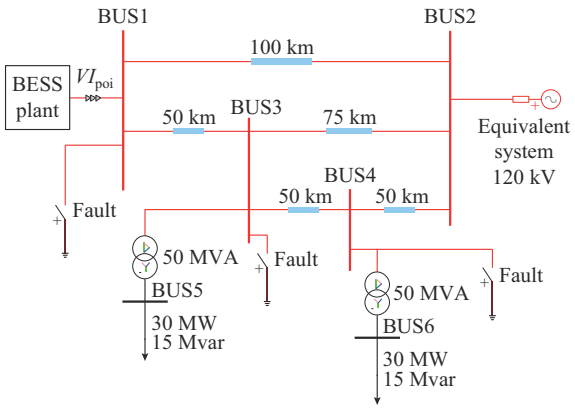

Fig. 8. Diagram of 75 MVA BESS plant connected to 120 kV/60 Hz transmission network.

The BESS plant is located at BUS1. The BESS plant model has a total nominal apparent power of 75 MVA. The main values of simulation parameters are provided in Table AI in Appendix A.

Each battery has a different initial SOC to analyze the efficiency of the proposed FRT control strategy to correctly han-

dle the discrepancies in battery SOCs. Furthermore, the model considers the tolerances on DC-link voltage measurement between the parallel-connected BDC units. This is important to demonstrate the benefits as well as the efficiency of the droop control solution for DC-link management when multiple BDC units are operated in parallel and controlling DC-link voltage.

At fault inception, the BESS plant absorbs $Q_{poi}=0.1$ p.u.. Double line-to-ground faults are applied at BUS1, BUS3s or BUS4, which are applied at $t=2$ s and removed at $t=2.5$ s. In all of the analyzed scenarios, the voltage and fault duration at the POI fall within the region, where the BESS must remain connected to the power grid according to the low-voltage ride through (LVRT) requirement of German grid code for a two-phase fault as shown in Fig. 9 [15].

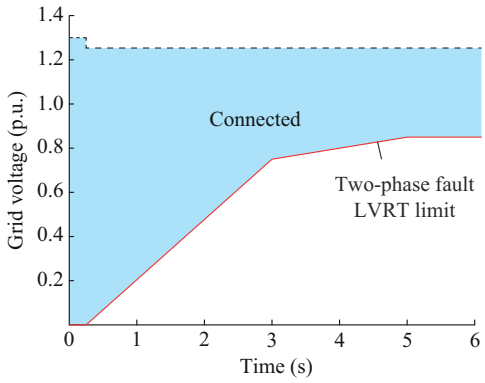

Fig. 9. LVRT requirement of German grid code for a two-phase fault.

III. Analysis of BESS with Proposed FRT Control Strategy

A. Validation of Performance of Proposed FRT Control Strategy on DC-link Management

As introduced in Section II-C, the proposed FRT control strategy includes changing the control of the BDC units and the GSC during FRT. At FRT activation, the BDC units transfer from constant battery current i_b control to constant DC-link voltage v_{dc} control through a droop structure based on measuring i_{dc}. The GSC transfers from outer loop constant v_{dc} control to constant control of i_{dg}^{+}. When the FRT controller detects that the grid voltage recovers to be within the limits, the BDC units automatically revert to constant i_b control and the GSC controller reverts to constant v_{dc} control.

The performance of the proposed FRT control strategy on DC-link management is compared with constant charging current control in Fig. 10. For this investigation, battery 1 has an initial SOC of 90% and battery 2 has an initial SOC of 20%. The initial power level of BESS plant is set as $p_0=0.75$ p.u.. The two-phase fault is applied at BUS4 with $K_{V\_}=2$. These results confirm that BDC DC-link voltage control can significantly reduce the transient voltage drop at fault inception as well as rapidly bring the DC-link voltage back within the range in steady state. Furthermore, the droop control also ensures proper current sharing between the BDC units as well as prevents the increase of i_{dc} in the BDC unit which supplies the battery with the lowest SOC. This approach also reduces the recovery time at fault removal as shown in Fig. 10. It is also worth mentioning that further investigations show that the proposed FRT control strategy also improves DC-link voltage control in discharging mode which reduces the use of the chopper during FRT. This requires tuning the BDC controller settings as well as the droop parameters.

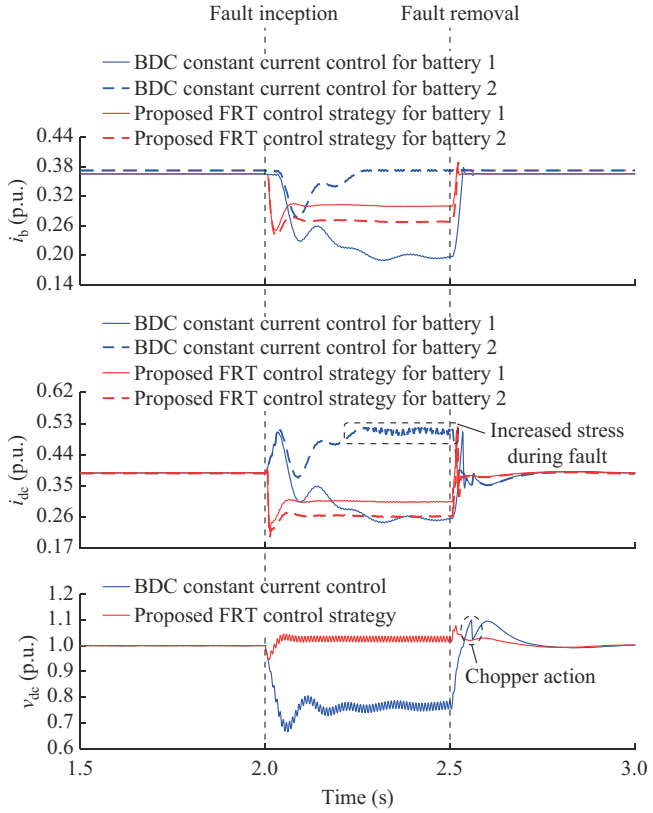

Fig. 10. Simulation validation of performance of proposed FRT control strategy on DC-link management with $N_{BDC}=2$.

B. Robustness Validation of Proposed FRT Control Strategy

The robustness of the proposed FRT control strategy to different grid code requirements, the severity of the grid fault, and the initial operating conditions of BESS plant are validated in this subsection.

The results in Fig. 11 show the BESS plant response to the minimum and maximum values of $K_{V\_}$ according to the German grid code [15], i. e., $K_{V\_}=2$ and $K_{V\_}=6$. For this validation, both of battery 1 and battery 2 have an initial SOC of 80%. The initial power of BESS plant is set as p_0 = 0.95 p.u. and the two-phase fault is applied at BUS4.

In both cases, the results show that no chopper action is required at fault removal. The results also show that a higher value of $K_{V\_}$ leads to increased injections of both i_{qg}^{-} and i_{dg}^{-}, which reduces the level of i_{dg}^{+} to continue charging the battery at the same rate.

The results in Fig. 11 also show that the BDC controller automatically reduces i_b at an appropriate level for each battery to maintain the power balance on the DC-link, such that

v_{dc} is properly regulated during the fault. It also shows that the BESS plant properly recovers to pre-fault conditions at fault removal as required by grid code. This confirms that the proposed control strategy is tolerant to the negative-sequence injection requirement of the German grid code. A similar conclusion can be drawn on K_{V+} since i^{+}_{qg} also limits the control of i^{+}_{dg}.

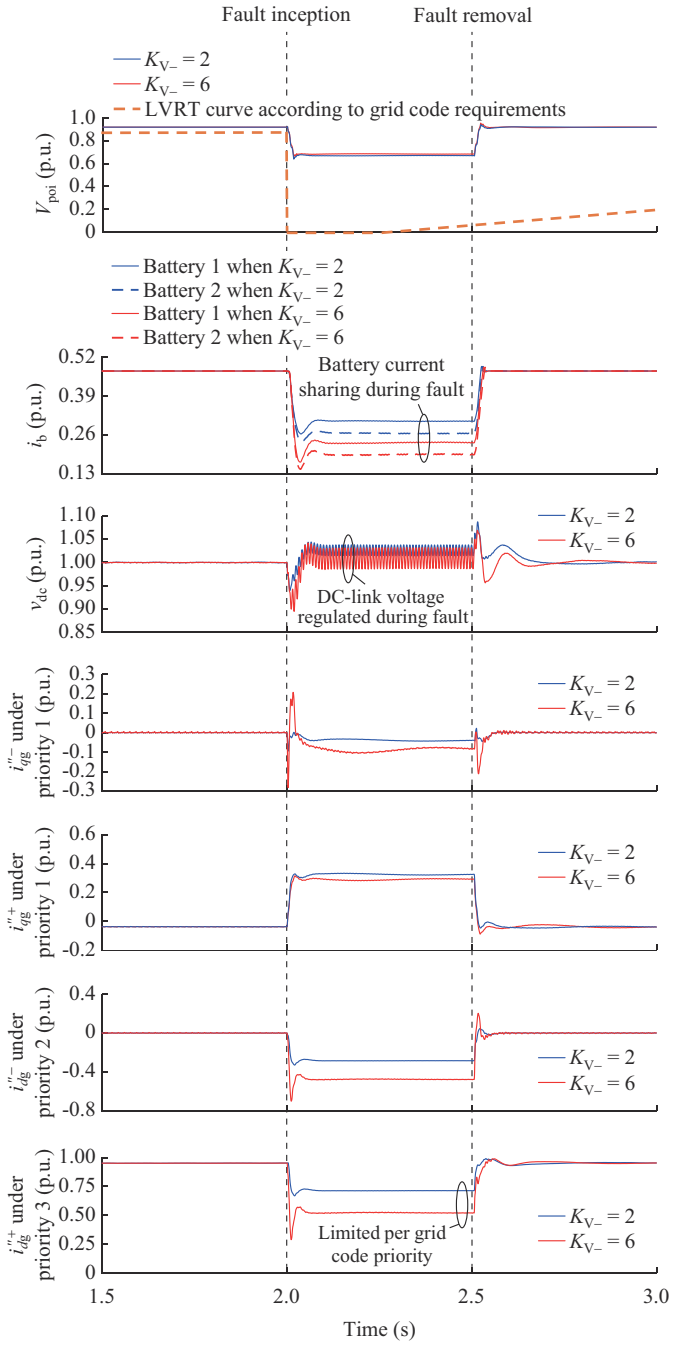

Fig. 11. Simulation validation of robustness of proposed FRT control strategy to grid code priority K_{V-} when $N_{BDC} = 2$.

Furthermore, the results in Fig. 12 show a comparison of the BESS plant response for a fault at BUS1, BUS3, and BUS4 under similar pre-fault conditions. For this validation, battery 1 has an initial SOC of 90% and battery 2 has an initial SOC of 20%. The initial power level of BESS plant is set as $p_0 = 0.75$ p.u.; and $K_{V-} = 2$.

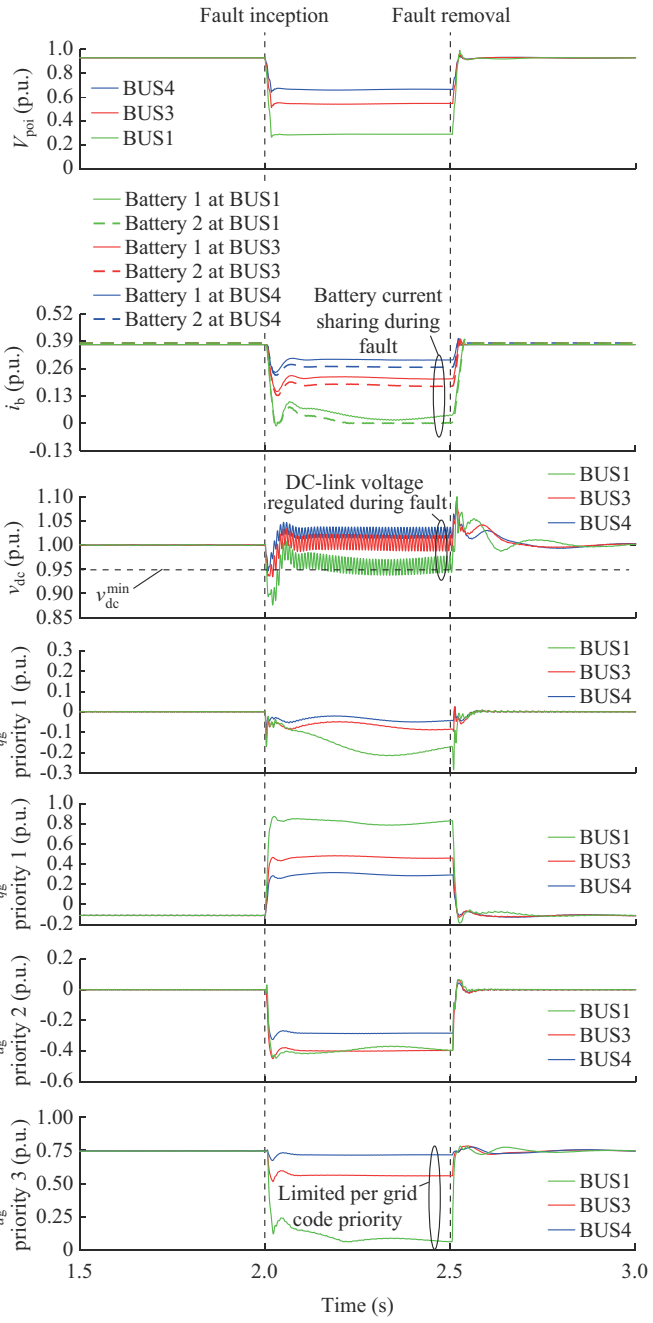

Fig. 12. Simulation validation of robustness of proposed FRT control strategy to fault severity when $N_{BDC} = 2$.

For the faults at BUS3 and BUS4, the results show that no chopper action is required at fault removal.

For a fault at BUS1, the chopper is activated once at fault removal. For a fault at BUS1, low-frequency oscillation is due to PLL transient response.

As expected, the voltage drop at the POI is also the most severe for a fault at BUS1. The results show that a closer fault at BUS1 or BUS3 leads to increased injections of i^{-}_{qg}, i^{+}_{qg}, and i^{-}_{dg}, which significantly limits the amount of i^{+}_{dg} absorbed by the GSC according to the grid code priority. For a

fault at BUS1, the available quantity of i_{dg}^{+} is almost zero. The results also show that i_b is reduced as required for each battery so that v_{dc} is properly regulated during the fault. For a fault at BUS1, it is also noted that the total battery current must be significantly reduced to maintain $v_{dc,min}$.

The results also show that the current in battery 2 eventually decreases to zero due to the low available quantity of i_{dg}^{+}. In a worst-case fault scenario, i_{dg}^{+} decreases to zero. In this case, the current decreases to zero in all batteries and the BESS plant naturally stops charging the batteries according to grid code priority (not shown). The results also show that the BESS plant properly recovers to pre-fault conditions following the fault removal according to grid code priority. This confirms that the proposed control strategy is also tolerant to the fault severity.

Finally, the results in Fig. 11 show the system response when both batteries have an initial SOC of 80%, and the BESS plant has an initial active power set-point of $p_0=0.75$ p.u.. The results in Fig. 12 show the system response under a different set of operating conditions. The initial SOCs of battery 1 and battery 2 are 90% and 20%, respectively, and the initial active power set-point of the BESS plant is $p_0=0.95$ p.u.. Since the proposed FRT control strategy permits proper FRT operation in all the cases analyzed in Fig. 11 and Fig. 12, it is also concluded that the proposed FRT control strategy is tolerant to initial operating conditions of BESS plant such as battery SOC and active power set-point.

C. Analysis on Importance of Droop Control

The main objective of the droop control is to adapt v'_{dc} to properly share the current among all the BDC units in parallel. Ideally, they should share equally the total charging current on the DC-link, i.e., $i_{dc}=i_{gsc}/N_{BDC}$, given that they have the same v'_{dc}. However, in practice, system discrepancies such as the tolerances on voltage feedback measurements can drive some BDC controllers into saturation, while other BDC units do not contribute to maintaining v_{dc}. The importance of the droop structure on charging current sharing is shown in Fig. 13. For this analysis, both battery 1 and battery 2 have an initial SOC of 80%. The initial power level of BESS plant is set as $p_0=0.95$ p.u.. The error on voltage measurement is $K_e=1$ for battery 1 and $K_e=0.99$ for battery 2. The two-phase fault is applied at BUS4.

The tolerance on DC-link voltage measurement can be modeled as an additional gain K_e in the voltage feedback measurement circuit, as shown in Fig. 14. The control design equation is given as:

$$e_v=v_{dc}^{min}+R_d i_{dc}-K_e v_{dc} \tag{24}$$

The objective of outer DC-link voltage controller of the BDC is to have $e_v=0$. Since v_{dc}^{min} and v_{dc} should be identical for all parallel BDC units, if $K_e<1$, then, according to (24), the term $R_d i_{dc}$ must be decreased, such that v'_{dc} decreases to compensate the error introduced by $K_e<1$. Since R_d is a fixed parameter, i_{dc} and i_b will both naturally decrease following the action of outer DC-link voltage controller of the BDC. The behavior is opposite if $K_e>1$.

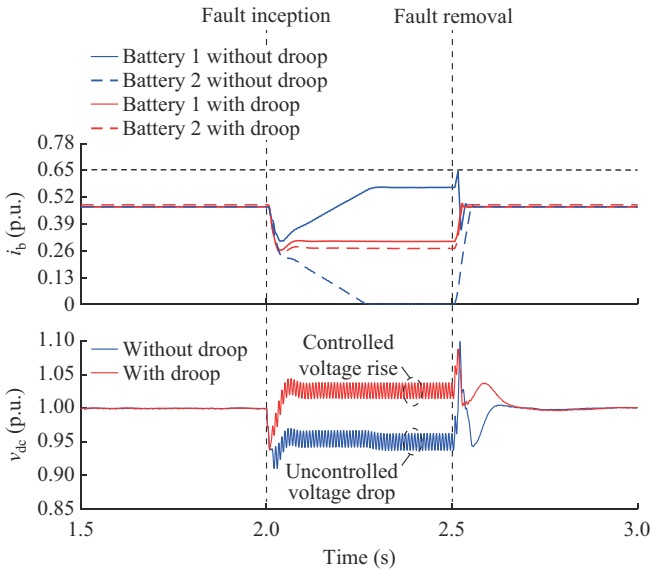

Fig. 13. Simulation results showing benefits of droop control on charging current sharing with $N_{BDC}=2$.

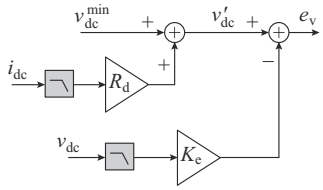

Fig. 14. Droop control with K_e on DC-link voltage measurement.

The second objective of the droop control is to adapt v'_{dc} to stabilize v_{dc}. In the charging mode, the parallel BDC units all act as loads as can be observed from the DC-link. For example, if v_{dc} decreases, it means that i_{dc} is too high compared with the current injected by the GSC i_{gsc}. Positive droop control is used to naturally increase v'_{dc} to decrease the value of i'_b sent to the BDC inner loop current controller. The behavior is opposite if the DC-link voltage increases. As shown in Figs. 10-13, proper droop settings can significantly reduce the transient voltage drop at fault inception and the overvoltage at fault removal.

In Fig. 15, the performance of the proposed FRT control strategy to properly manage the DC-link during grid fault is also validated with a higher number of BDC units in parallel ($N_{BDC}=4$) with each battery having a different initial SOC and each BDC having a different K_e on its voltage feedback measurement. While R_d is kept the same as for the previous scenarios with $N_{BDC}=2$, R_d can be tuned as needed to improve both current sharing and DC-link voltage level. For this validation, battery 1 has an initial SOC of 20%, battery 2 of 40%, battery 3 of 60%, and battery 4 of 80%. The error on voltage measurement is K_e=1.01 for battery 1, K_e=1.00 for battery 2, $K_e=0.99$ for battery 3, and $K_e=0.98$ for battery 4. The initial power level of BESS plant is set as $p_0=0.95$ p.u.; and $K_{V\_}=2$. The two-phase fault is applied at BUS3.

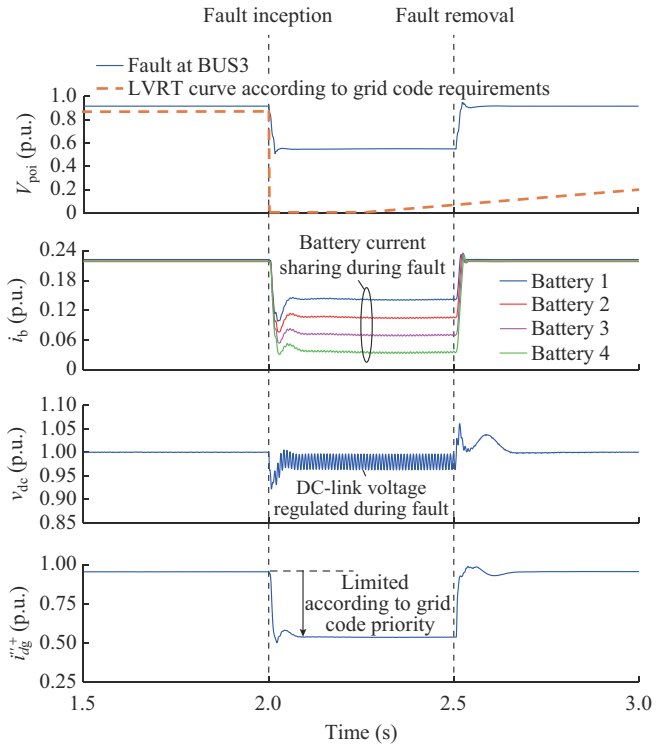

Fig. 15. Simulation validation of proposed FRT control strategy with a higher number of BDC units in parallel ($N_{BDC} = 4$).

IV. Conclusion

Operating a BESS plant under conventional constant charging current control may lead to inadequate DC-link management under stringent unbalanced grid fault conditions. This problem is aggravated with a flexible positive- and negative-sequence control scheme compliant with the German grid code [15] requirements and with multiple batteries connected to the same DC-link through BDC units. Inadequate DC-link regulation can in turn prevent BESS plants from complying with emerging grid code requirements on additional reactive current in the positive- and negative-sequence systems.

The contribution of this paper is the proposal of a new FRT control strategy for compliance of practical BESS plants with emerging grid codes such as the German grid code in charging mode. The proposed control strategy consists of adapting the controls of the BDC units and GSC upon receiving an FRT activation signal. At FRT activation, the BDC units switch from constant battery current control mode to constant DC-link voltage control mode through a droop structure. The GSC switches from constant DC-link voltage control mode to constant positive-sequence active current control mode. The control priority is equally given to negative- and positive-sequence reactive current control according to the grid code priority. When the AC voltage returns to the normal operation region, the BDC and GSC controllers automatically revert to their initial controls. The proposed control strategy is tolerant to initial operating conditions of BESS plant, grid code requirements as well as fault severity, and ensures the minimum perturbation on the DC-link.

Appendix A

TABLE AI
Main Values of Simulation Parameter

	Parameter	Value
BESS plant	Nominal grid voltage (root mean square)	120 kV
	Nominal grid frequency	60 Hz
	P_{BESS}	1.5 MW
	S_{BESS}	1.67 MVA
	N_{BESS}	45
	N_{BDC}	2 or 4
	Total nominal active power	75 MW
	FRT pickup voltage	0.85 p.u.
	FRT reset voltage	0.85 p.u.
	Initial reactive power absorbed $\lvert Q'_{poi} \rvert$	0.1 p.u.
DC-link	V_{dc}	1150 V
	v_{dc}^{ref}	1.0 p.u.
	$V_{dc,on}$	1.1 p.u.
	$V_{dc,off}$	1.025 p.u.
	Total DC-link capacitance	1.7 F
GSC	K_{V+}	2
	I_{dg}^{lim}	1.0 p.u.
	I_{qg}^{lim}	1.0 p.u.
	I_{g}^{lim}	1.1
BDC	L_b	0.33 mH
	R_d	5 mΩ
	v_{dc}^{min}	0.95 p.u.
Battery	Q_n	29.35 kAh ($N_{BDC}=2$) 14.68 kAh ($N_{BDC}=4$)
	V_n	805 V
	A	68 V
	B	0.0019 Ah^{-1} ($N_{BDC}=2$) 0.0023 Ah^{-1} ($N_{BDC}=4$)
	R_s	0.274 mΩ ($N_{BDC}=2$) 0.549 mΩ ($N_{BDC}=4$)
	K	0.00015 V/Ah ($N_{BDC}=2$) 0.00030 V/Ah ($N_{BDC}=4$)
	E_0	870 V
	T_n	1 hour

References

[1] R. Hemmati and H. Mehrjerdi, "Stochastic linear programming for optimal planning of battery storage systems under unbalanced-uncertain conditions," *Journal of Modern Power Systems and Clean Energy*, vol. 8, no. 5, pp. 971-980, Sept. 2020.

[2] F. Wu, B. Yang, and J. Ye, *Grid-scale Energy Storage Systems and Applications*. New York: Academic Press, 2019.

[3] S. Vazquez, S. M. Lukic, E. Galvan *et al.*, "Energy storage systems for transport and grid applications," *IEEE Transactions on Industrial Electronics*, vol. 57, no. 12, pp. 3881-3895, Dec. 2010.

[4] X. Li, L. Yao, and D. Hui, "Optimal control and management of a large-scale battery energy storage system to mitigate fluctuation and intermittence of renewable generations," *Journal of Modern Power Systems and Clean Energy*, vol. 4, no. 4, pp. 593-603, Oct. 2016.

[5] A. J. Sangster, "Massive energy storage systems enable secure electricity supply from renewables," *Journal of Modern Power Systems and Clean Energy*, vol. 4, no. 4, pp. 659-667, Oct. 2016.

[6] L. Yao, B. Yang, H. Cui *et al.*, "Challenges and progresses of energy storage technology and its application in power systems," *Journal of Modern Power Systems and Clean Energy*, vol. 4, no. 4, pp. 519-528,

Oct. 2016.
[7] *IEEE Guide for Design, Operation and Maintenance of Battery Energy Storage Systems, both Stationary and Mobile, and Applications Integrated with Electric Power Systems*, IEEE Std 2030.2.1, 2019.
[8] *IEEE Standard Test Procedures for Electric Energy Storage Equipment and Systems for Electric Power Systems Applications*, IEEE Standard 2030.3-2016, 2016.
[9] *IEEE Recommended Practice for the Characterization and Evaluation of Energy Storage Technologies in Stationary Applications*, IEEE Standard 1679-2020, 2020.
[10] U. Karaagac, J. Mahseredjian, R. Gagnon *et al.*, "A generic EMT-type model for wind parks with permanent magnet synchronous generator full size converter wind turbines," *IEEE Power and Energy Technology Systems Journal*, vol. 6, no. 3, pp. 131-141, Sept. 2019.
[11] S. Wang, P. Dehghanian, M. Alhazmi *et al.*, "Advanced control solutions for enhanced resilience of modern power-electronic-interfaced distribution systems," *Journal of Modern Power Systems and Clean Energy*, vol. 7, no. 4, pp. 716-730, Jul. 2019.
[12] M. Chen, D. Zhou, and F. Blaabjerg, "Modelling, implementation, and assessment of virtual synchronous generator in power systems," *Journal of Modern Power Systems and Clean Energy*, vol. 8, no. 3, pp. 399-411, May 2020.
[13] IEEE, "Impact of inverter-based generation on bulk power system dynamics and short-circuit performance," NERC Task Force on Short-Circuit and System Performance Impact of Inverter Based Generation, Palo Alto, USA, Tech. Rep. TR68, Jul. 2018.
[14] A. Hooshyar, M. A. Azzouz, and E. F. El-Saadany, "Distance protection of lines emanating from full-scale converter-interfaced renewable energy power plants–part I: problem statement," *IEEE Transactions on Power Delivery*, vol. 30, no. 4, pp. 1770-1780, Aug. 2015.
[15] *Technische Regeln den Anschluss von Kundenanlagen an das Hochspannungsnetz und Deren Betrieb (TAR Hochspannung)*, VDE-AR-N 4120 Anwendungsregel, Oct. 2018.
[16] A. Haddadi, M. Zhao, I. Kocar *et al.*, "Impact of inverter-based resources on negative sequence quantities-based protection elements," *IEEE Transactions on Power Delivery*, vol. 36, no. 1, pp. 289-298, Feb. 2021.
[17] P. Rodrigue, J. Pou, J. Bergas *et al.*, "Decoupled double synchronous reference frame PLL for power converters control," *IEEE Transactions on Power Electronics*, vol. 22, no. 2, pp. 584-592, Mar. 2007.
[18] M. Swierczynski, R. Teodorescu, C. N. Rasmussen *et al.*, "Overview of the energy storage systems for wind power integration enhancement," in *Proceedings of 2010 IEEE International Symposium on Industrial Electronics (ISIE)*, Bari, Italy, Jul. 2010, pp. 3749-3756.
[19] C. Abbey and G. Joos, "Supercapacitor energy storage for wind energy applications," *IEEE Transactions on Industry Applications*, vol. 43, no. 3, pp. 769-776, Jun. 2007.
[20] L. Huchel, M. S. El Moursi, and H. H. Zeineldin, "A parallel capacitor control strategy for enhanced FRT capability of DFIG," *IEEE Transactions on Sustainable Energy*, vol. 6, no. 2, pp. 303-312, Apr. 2015.
[21] H. S. Krishnamoorthy, D. Rana, P. Garg *et al.*, "Wind turbine generator –battery energy storage utility interface converter topology with medium-frequency transformer link," *IEEE Transactions on Power Electronics*, vol. 29, no. 8, pp. 4146-4155, Aug. 2014.
[22] F. M. Gatta, A. Geri, S. Lauria *et al.*, "Modelling of battery energy storage systems under faulted conditions: assessment of protection systems behaviour," in *Proceedings of International Conference on Environmental and Electrical Engineering (EEEIC)*, Florence, Italy, Jun. 2016, pp. 1-6.
[23] A. Neves, B. Almeida, M. Louro *et al.*, "Protection scheme for energy storage systems operating in island or grid-connected modes," *CIRED-Open Access Proceedings Journal*, vol. 2017, no. 1, pp. 1-5, Oct. 2017.
[24] Y. Bak, J.-S. Lee, and K.-B. Lee, "A low voltage ride through control strategy for energy storage systems," in *Proceedings of IEEE Energy Conversion Congress and Exposition (ECCE)*, Milwaukee, USA, Sept. 2016, pp. 1-6.
[25] H. Wang, Q. Zhang, D. Wu *et al.*, "Advanced current-droop control for storage converters for fault ride-through enhancement," *IEEE Journal of Emerging and Selected Topics in Power Electronics*, vol. 8, no. 3, pp. 2461-2474, Sept. 2020.
[26] M. Ozbek, B. Pierquet, and A.D. Baglino, "Scalable and flexible cell-based energy storage system," U.S. Patent US20170093156A1, Sept. 3, 2021.
[27] EPRI, "Battery energy storage systems modeling for short-circuit studies," Palo Alto, USA, Tech. Rep. TR-3002018696, 2020.
[28] M. Berger, I. Kocar, E. Farantatos *et al.*, "Modeling of li-ion battery energy storage systems (BESSs) for grid fault analysis," *Electric Power Systems Research*, vol. 196, pp. 1-6, Jul. 2021.
[29] Y. Liu and Y. Luo, "Search for an optimal rapid-charging pattern for li-ion batteries using the Taguchi approach," *IEEE Transactions on Industrial Electronics*, vol. 57, no. 12, pp. 3963-3971, Dec. 2010.
[30] O. Tremblay and L. A. Dessaint, "Experimental validation of a battery dynamic model for EV applications," *World Electric Vehicle Journal*, vol. 3, no. 1, pp. 1-10, Jan. 2009.
[31] S. Bacha, I. Munteanu, and A. I. Bratcu, "Linear control approaches for DC-DC power converters," in *Power Electronic Converters Modeling and Control*. New York: Springer, 2014, pp. 55-96.
[32] T. Kauffmann, U Karaagac, I. Kocar *et al.*, "Short-circuit model for type-IV wind turbine generators with decoupled sequence control," *IEEE Transactions on Power Delivery*, vol. 34, no. 5, pp. 1998-2007, Oct. 2019.
[33] T. Kauffmann, U Karaagac, I. Kocar *et al.*, "An accurate type III wind turbine generator short circuit model for protection applications," *IEEE Transactions on Power Delivery*, vol. 32, no. 6, pp. 2370-2379, Dec. 2017.
[34] A. Haddadi, I. Kocar, T. Kauffmann *et al.*, "Field validation of generic wind park models using fault records," *Journal of Modern Power Systems and Clean Energy*, vol. 7, no. 4, pp. 826-836, Jul. 2019.

Maxime Berger received the B.Eng. degree from the Université du Québec à Rimouski, Rimouski, Canada, in 2014, and the M.A.Sc. and Ph.D. degrees in electrical engineering from Polytechnique Montréal, Montréal, Canada, in 2016 and 2019, respectively. From 2012 to 2021, he was with Bombardier Transportation, St.-Bruno, Canada, where he has been involved in the development and integration of auxiliary systems for electrical transportation applications. He is currently an Assistant Professor in electrical engineering at the Université du Québec à Rimouski. His research interests include grid integration of renewable energy, power system protection, and simulation and analysis of power systems transients.

Ilhan Kocar received the B.Sc. and M.Sc. degrees in electrical and electronics engineering from Orta Doğu Teknik Üniversitesi, Ankara, Turkey, in 1998 and 2003, respectively, and the Ph.D. degree in electrical engineering from Polytechnique/Université de Montréal, Montréal, Canada, in 2009. He worked as a Project Engineer at Aselsan Electronics Inc., Ankara between 1998 and 2004. He worked as a Distribution Software R&D Engineer at CYME International T&D, St-Bruno between 2009 and 2011. He joined the faculty at Polytechnique Montreal in 2011. His career highlights include major contributions to professional simulation tools, and development of solutions for large-scale integration of inverter-based resources (IBRs). He has performed many research and grid-consulting projects that cover design, rigorous mathematical modeling, analysis, and validation of field measurements.

Evangelos Farantatos received the Diploma in electrical and computer engineering from the National Technical University of Athens, Athens, Greece, in 2006 and the M.S. and Ph.D. degrees from the Georgia Institute of Technology, Atlanta, USA, in 2009 and 2012, respectively. He is a Senior Project Manager with the Grid Operations and Planning R&D Group at EPRI, Palo Alto, USA. His research interests include synchrophasor technology, power systems monitoring and control, power system stability and dynamics, renewable energy resource modeling, grid operation and protection with high level of inverter-based resources.

Aboutaleb Haddadi received the B.Sc. and M.Sc. degrees in electrical engineering from Sharif University of Technology, Tehran, Iran, in 2007 and 2009, respectively, and the Ph.D. degree in electrical engineering from McGill University, Montréal, Canada, in 2015. From 2015 to 2020, he was a Research Associate with Polytechnique Montréal, Montréal, Canada. Since 2020, he has been a Senior Engineer Scientist with the Grid Operations and Planning R&D Group at EPRI. He has consulting experience in the area of power system transients and simulation. Dr. Haddadi is active in a number of IEEE Power System Relaying and Control Committee, IEEE PES, and CIGRE working groups and is currently leading CIGRE Working Group C4.60 on Generic EMT Modeling of Inverter-Based Resources for Long Term Planning Studies. His research interests include grid integration of renewable energy, transmission system protection and impact of renewable energy, and power system modeling and simulation.